

34 Angrites are defined as a group of unshocked, alkali-depleted basaltic meteorites that
35 are amongst the oldest igneous rocks in the Solar System^{1,2}. Based on the mineral chemistry of
36 pyroxene (Fe/Mn ratios) within angrites and the isotopic dichotomy between non-
37 carbonaceous and carbonaceous chondrites, it is likely that angrites originate from the inner
38 Solar System^{3,4}. Evidence from Mn/Cr isotopic systematics indicates that the angrite parent
39 body (APB) was larger than the asteroid 4Vesta⁵. On the basis of differing textures and
40 mineralogy, angrites have been principally divided into plutonic angrites (slowly cooled) with
41 crystallisation ages ranging from 4560.74 ± 0.47 Ma to 4556.60 ± 0.26 Ma and quenched
42 angrites (rapidly cooled) with crystallisation ages ranging from 4564.39 ± 0.24 Ma to 4562.2
43 ± 0.7 Ma⁵. However, there are some angrites, with similar mineralogical assemblages yet
44 differing textures, which do not fit into either of these categories. For example, Northwest
45 Africa (NWA) 8535 has been classified as a dunite (early formed cumulate) and NWA 10463
46 represents an intermediate type between the plutonic and quenched angrites, which has recently
47 been dated at 4560.25 ± 0.18 Ma^{6,7}.

48
49 The oxygen isotope compositions of bulk angrites have previously been reported as
50 displaying a high level of homogeneity, particularly with regards to ¹⁷O-excess ($\Delta^{17}\text{O}$),
51 indicating that all the currently identified angritic meteorites originated from a single parent
52 body and likely underwent early isotopic homogenisation in a global magma ocean^{8,9}.
53 Although many angrites display limited evidence of shock deformation, indicating that the
54 APB was not affected by multiple impact events¹⁰, it has been suggested that the quenched
55 angrites may represent impact melts^{11,12}. While this hypothesis has been disputed¹, the recent
56 discovery of variable deformation features in olivine xenocrysts within Asuka (A)-881371 and
57 A 12209 further support the impact hypothesis^{13,14}, whereby olivine xenocrysts are relict grains
58 originating from areas of the APB that survived impact melting¹³. However, it has also been
59 argued that the kink bands and sub-grain boundary formation in olivine grains could result
60 from ductile deformation in the APB mantle¹⁴. Consequently, further work is required to
61 constrain the petrogenesis of the quenched angrites.

62
63 We collected high-precision, oxygen three-isotope data on bulk-rock samples from nine
64 angrites, encompassing all petrologic subgroups (Supplementary Figure 1), using laser-assisted
65 fluorination following established procedures^{9,15}. In addition, separated olivine and
66 groundmass fractions from A-881371, A 12209, and NWA 12320 were also analysed for their
67 oxygen isotopic composition. All samples were treated with a solution of ethanolamine

68 thioglycollate (EATG) to ensure that any isotopic variations were not a result of terrestrial
69 contamination (Supplementary Figure 4). For the whole-rock analysis of NWA 12320 ($n = 2$)
70 we report the typical uncertainty of oxygen isotopic analyses at ± 0.018 ‰, as demonstrated
71 by replicate analyses of homogenous standards¹⁶. All uncertainties for averages and the AFL
72 (angrite fractionation line) are reported at 2SD.

73

74 **Results**

75 While the oxygen isotopic compositions ($\Delta^{17}\text{O}$ see methods for calculation) for five
76 angrites have been previously reported as homogenous ($\Delta^{17}\text{O} = -0.072 \pm 0.014$ ‰⁸), we
77 observe that the $\Delta^{17}\text{O}$ values of whole-rock NWA 12320 ($\Delta^{17}\text{O} = -0.024 \pm 0.018$ ‰) and the
78 average $\Delta^{17}\text{O}$ of groundmass fractions of NWA 12320, A 12209 and A-881371 ($\Delta^{17}\text{O} = -0.003$
79 ± 0.020 ‰ $n = 8$) are less negative, and are statistically distinct from the other angrites (Figure
80 1, Table Supplementary 1 & 2). Intriguingly, the olivine xenocrysts in NWA 12320, A 12209
81 and A-881371 display an average $\Delta^{17}\text{O}$ value ($\Delta^{17}\text{O} = -0.068 \pm 0.014$ ‰ $n = 8$)
82 indistinguishable from the other whole-rock angrite meteorites (Figure 1, Table Supplementary
83 1 & 2). These results indicate that the groundmass in NWA 12320, A 12209 and A-881371 are
84 isotopically distinct from the rest of the sample. While lesser amounts of groundmass may
85 result in undetectable shifts in some quenched angrites, NWA 12320 is dominated by
86 groundmass and therefore the whole-rock sample equates to a groundmass separate. The origin
87 of such isotopic heterogeneity within magmatic samples requires the addition of isotopically
88 distinct material. Therefore, to calculate an angrite fractionation line (AFL) we have opted to
89 incorporate the $\Delta^{17}\text{O}$ values of the olivine xenocrysts in NWA 12320, A 12209 and A-881371,
90 as they formed prior to the groundmass and so pre-date the introduction of any additional
91 isotopically anomalous material. We have excluded the groundmass fractions and the whole-
92 rock value of NWA 12320. From this, we derive an average $\Delta^{17}\text{O}$ value of -0.066 ± 0.016 ‰,
93 redefining the AFL utilising eleven individual samples. All whole-rock measurements reported
94 here, excluding the groundmass-dominated NWA 12320 datum, fall within the uncertainty of
95 this new AFL, providing evidence that angrites are homogenous in regard to $\Delta^{17}\text{O}$ and
96 suggesting that angrite meteorites originate from a single differentiated parent body that was
97 homogeneous with respect to oxygen isotopes.

98

99 **Thermal processing of relict olivine grains**

100

101 Xenocrysts in NWA 12320 have had a complex history as shown from contrasting
102 internal structures revealed by electron backscatter diffraction (EBSD) data and point to two
103 distinct populations of olivine xenocrysts, one of which has a granular texture, clearly
104 illustrated by band contrast images and inverse pole figures (IPF) (Figure 2a-c). The granular
105 olivine xenocrysts have no discernible preferred orientation and are cemented by olivine with
106 a higher Fe content, with each neighbouring grains displaying vastly distinct orientations. This
107 is indicative of recrystallization, after shock-induced mosaicism or fragmentation. A second
108 population of olivine xenocrysts demonstrates unaltered, undeformed grains with little to no
109 internal misorientation (Figure 2d-f). A similarly complex history for the xenocrysts within A
110 12209 is exhibited by various degrees of lattice deformation, from weak deformation bands to
111 sub-grain rotation crystallization (Supplementary Figure 2).

112

113 **Discussion**

114

115 The granular textures seen in NWA 12320 resemble experimental recrystallization
116 textures induced at 1000 °C under dynamic conditions¹⁷, but are also similar to polycrystalline
117 olivine identified in the howardite impact melt breccia Jiddat al Harasis (JaH) 556¹⁸ and the
118 ureilite impact melt breccia Jiddat al Harasis 422¹⁹. Most noticeably, there is a measurable
119 oxygen isotope variation between the groundmass and the whole-rock values for both samples,
120 similar to those observed in this study for the quenched angrite meteorites. In the case of JaH
121 556 and JaH 422 it was concluded that the olivine xenocrysts represent relict grains that
122 underwent recrystallisation in the impact melt. This indicates that xenocrysts within NWA
123 12320, A 12209 and A-881371 are in fact relict olivines grains that were affected by high-
124 temperature processes. The identification of angrite-like clasts in howardites, various polymict
125 urelites and CH3 chondrites lends additional support for the proposition that the APB was
126 subjected to impact processing^{20,21,22,23}. Moreover, the metal identified within the plutonic
127 angrite NWA 2999 has been previously attributed to an exogenous source, introduced by
128 impact events²⁴. Thus, there is considerable evidence to support impact mixing on the APB
129 early in Solar System history. The lack of shock deformation features within other relict olivine
130 grains, plutonic, intermediate and dunitic angrites may reflect the greater depth at which these
131 angrites formed or that they were more distal to the impact site(s) (Figure 3). Additionally, the
132 chronological separation between the quenched angrites and plutonic angrites implies that the
133 plutonic angrites had either not formed or were still molten at the time of impact, and therefore
134 did not experience or preserve any shock-induced deformation.

135

136 While mantle rheology has been proposed as the cause of the variable deformation seen
137 in some relict olivines in angrites¹⁴, the oxygen isotopic disequilibrium we observe between
138 the olivine and groundmass indicates they have distinct origins. Our data clearly indicate that
139 the groundmass was the product of an impact event resulting in isotopic contamination by the
140 impactor, whereas the olivines represent relict material of the APB. The significant difference
141 in $\Delta^{17}\text{O}$ values between the groundmass and olivine, implies that the impactor formed in a
142 different region of the protoplanetary disk in relation to the APB. In a scenario analogous to
143 that proposed for JaH 556¹⁸, it would only require a small quantity of impactor material to
144 account for the isotopic disequilibrium displayed by groundmass and relict olivines, provided
145 the impactor was enriched in $\Delta^{17}\text{O}$ compared to the APB. It has been recently suggested that
146 angrites record mixing of inner and outer Solar System material (CI and CM carbonaceous
147 chondrites) based on their relatively elevated H and N isotopic compositions^{25,26}. However, the
148 CM chondrites have a more negative $\Delta^{17}\text{O}$ compared to angrites²⁷, and while CI chondrites are
149 slightly more positive in $\Delta^{17}\text{O}$, they also have extremely positive $\delta^{18}\text{O}$ values²⁷ and would
150 therefore not be capable of the isotopic shift in values observed in the quenched angrites
151 (Supplementary Figure 5). A chondritic impactor with a significantly positive $\Delta^{17}\text{O}$ value, such
152 as the ordinary or R chondrites might be proposed²⁸. However, a chondritic impactor would
153 result in significantly enriched siderophile elements, whereas angrites are well known for their
154 depletion in siderophile elements relative to chondrites^{29,30}. Rumuruti, for example, has a nickel
155 content of 14.4 mg/g³¹. When mixed with the APB (2.5 % impactor), one would expect ~360
156 ppm Ni, whereas A 881371 has ~103 ppm Ni²⁹. We must therefore conclude that the impactor
157 that struck the APB was differentiated, analogous to achondrite meteorites. To satisfy our
158 oxygen isotope constraints the impactor must have had $\Delta^{17}\text{O}$ significantly above the TFL. A
159 number of achondrites with $\Delta^{17}\text{O}$ values similar to the L chondrites have been identified
160 (Supplementary Table 3). Based on our data, an impactor with the oxygen isotopic composition
161 of these known achondrites would satisfy all the isotopic constraints. However, it must also be
162 recognised that the modern day asteroid belt is highly depleted compared with its likely early
163 Solar System mass³². Therefore, it is likely that this achondritic impactor has been destroyed
164 and does not exist in the modern Solar System.

165

166 Regardless of the impactor, the combination of oxygen isotopic disequilibrium and
167 evidence of high-temperature events causing recrystallization of relict olivine grains, provides

168 a compelling case for mixing early in Solar System history, and an impact melt origin for the
169 quenched angrite meteorites (Figure 3).

170

171 The terrestrial fractionation line (TFL) is commonly used as a graphical reference when
172 comparing distinct groups of extra-terrestrial samples and is normally quoted as having a $\Delta^{17}\text{O}$
173 value of 0‰. However, there is significant uncertainty about the exact $\Delta^{17}\text{O}$ value of the TFL,
174 as this is dependent on the nature of the physical and thermal conditions that affected the
175 reference sample suite used to define it³³. In addition, there is, so far no consensus about the
176 appropriate slope factor that should be used for silicate minerals when calculating $\text{D}^{17}\text{O}^{33}$.
177 Furthermore, it has been shown that terrestrial rocks and minerals form fractionation arrays
178 that display slight y-axis offsets of approximately -30 to -70 ppm on the Vienna Standard
179 Mean Ocean Water (VSMOW) reference scale³³. To define an appropriate terrestrial reference
180 line to compare our angrite samples with, we have recalculated the 195 terrestrial samples from
181 a previous study³³, using an identical slope value to that used for the angrites (0.5247) and
182 without an applied y-axis offset correction. This reference line is therefore directly comparable
183 with our angrite data and has a $\Delta^{17}\text{O}$ value of -0.048 ± 0.020 ‰. As the $\Delta^{17}\text{O}$ value of our
184 newly redefined AFL ($\Delta^{17}\text{O} = -0.066 \pm 0.017$ ‰) overlaps with the terrestrial mantle signature
185 (Figure 1) this could indicate that the APB formed from the same O-isotope reservoir as the
186 Earth, although differences in some nucleosynthetic isotope signatures between Earth and the
187 APB (e.g., $\epsilon^{48}\text{Ca}$, $\epsilon^{50}\text{Ti}$, $\epsilon^{54}\text{Cr}$ and $\epsilon^{62}\text{Ni}$) point to their distinct origins^{1,34}.

188

189 It has been suggested that the formation and migration of giant gas planets are crucial
190 to the evolution of planetary systems, yet the timing of these events in our Solar System remains
191 largely unconstrained³⁵. In addition to the major impact event required to explain the oxygen
192 isotope variability in angrites proposed here, CB chondrites are very ancient meteorites that
193 exhibit evidence of mixing with a differentiated body that could have been sourced from the
194 outer Solar System³⁵. Such extreme dynamical excitement is not an expected result of the
195 classical accretion of bodies, and demands the interference of the giant gas planets³⁵.

196

197 Currently, three main competing models exist to explain the evolution of the Solar
198 System, the ‘Grand Tack’, ‘Low-mass asteroid belt’ and ‘Early Instability models’³⁶. The
199 ‘Low-mass asteroid belt’ model relies on later dynamical evolution induced by the chaotic
200 evolution of Jupiter and Saturn³⁶, while the ‘Early Instability model’ suggests dynamical
201 excitement ~ 10 Ma after the dispersal of the gaseous disk³⁶. The evidence of large-scale mixing

202 in the first 2-3 Ma of Solar System history presented here is in support of the ‘Grand Tack’
203 model and argues against the later dynamical excitement suggested by the other two models.
204 The “Grand Tack” model of giant planet migration implies that Jupiter first migrates inwards
205 and then, as the result of a resonance with Saturn migrated outwards again³⁷. During the initial
206 inward drift, rocky planetesimals were scattered inwards to 1 AU or less. The disc here became
207 thickened and formed the feeder zones for Earth and Venus. However, a proportion (14 %) of
208 these rocky planetesimals were also scattered outwards to 3 AU and beyond³⁷. During
209 subsequent outward migration, some of this rocky material was encountered again by the giant
210 planets and scattered back into the inner main belt. Finally, towards the end of the Grand Tack,
211 the gas giants moved through the outer icy planetesimal zone, scattering a fraction of them
212 inwards into the main belt³⁷.

213

214 As previously noted, volcanic activity on the angrite parent body took place extremely
215 early in Solar System history, at around 4564 Ma⁵ and so, approximately 3 Ma after calcium-
216 aluminium-rich inclusion formation (4567.30 ± 0.16 Ma³⁸). This is within the 4 Ma period
217 during which the solar nebular gas is considered to have persisted³⁹. Impact dynamics within
218 the inner Solar System with gas still present would have been subdued compared to those that
219 prevailed after the nebula had dissipated. As a consequence, displacement of the APB from the
220 inner Solar System and implantation into the main belt appears to have taken place with only
221 low levels of deformation. If this model is correct, it suggests that angrites preserve an early
222 deformation record that is related to Jupiter’s inward and subsequent outward migration.
223 Consequently, the oxygen isotope disequilibrium recorded by the impact melt and relict olivine
224 grains in angrite meteorites may represent the earliest isotopic evidence for the Grand Tack
225 migration. The quenched angrite meteorite D’Orbigny is a commonly used Pb-Pb anchor due
226 to the previous suggestions that quenched angrites are primitive, unshocked, pristine samples⁴⁰.
227 However, we have now demonstrated that some quenched angrites have in fact suffered major
228 impact processing. While D’Orbigny does not appear to demonstrate measurable evidence of
229 impactor contamination in its whole-rock O-isotope composition, the similarity in textures and
230 chemical compositions with the A 12209, A-881371 and NWA 12320 samples strongly
231 indicates a common origin. Any adjustments to the time anchor would require a corresponding
232 correction to the ‘model ages’ of all materials dated using D’Orbigny as an anchor. This, in
233 turn, has consequences for accurately defining the absolute timeline of Solar System events.

234

235

236 **Methods**

237 Oxygen isotope analyses were undertaken by laser-assisted fluorination at The Open
238 University, UK following established procedures^{8,15}. Oxygen isotopic analyses are given in
239 standard δ notation, where $\delta^{18}\text{O}$ is calculated relative to the international standard, Vienna
240 Standard Mean Ocean Water (VSMOW) as:

241

$$242 \quad \delta^{18}\text{O} = [({}^{18}\text{O} / {}^{16}\text{O}_{\text{sample}}) / ({}^{18}\text{O} / {}^{16}\text{O}_{\text{VSMOW}}) - 1] \times 1000 \text{ (‰)}$$

243

244 and similarly, for $\delta^{17}\text{O}$ using the ${}^{17}\text{O} / {}^{16}\text{O}$ ratio.

245

246 $\Delta^{17}\text{O}$ represents the deviation of a sample, or group of samples, from the terrestrial
247 fractionation line (TFL) and has proved to be a useful parameter for defining different parent
248 body sources^{15,41}. In this paper all $\Delta^{17}\text{O}$ were calculated using the linearized format⁴² with $\lambda =$
249 0.5247.

250

$$251 \quad \Delta^{17}\text{O} = 1000 \ln(1 + \delta^{17}\text{O}/1000) - \lambda 1000 \ln(1 + \delta^{18}\text{O}/1000)$$

252

253

254 Laser-assisted fluorination currently provides the highest precision available for
255 oxygen isotope analysis. Replicate analyses of our internal obsidian standard (N = 38) gave the
256 following values: (2SD) of $\pm 0.053 \text{ ‰}$ ($\delta^{17}\text{O}$), $\pm 0.095 \text{ ‰}$ ($\delta^{18}\text{O}$), and $\pm 0.018 \text{ ‰}$ ($\Delta^{17}\text{O}$)¹⁶.
257 While laser fluorination does not provide spot analysis, unlike secondary ion mass
258 spectrometry (SIMS) or UV laser ablation, the need to resolve slight differences in $\Delta^{17}\text{O}$ means
259 that its ability to provide very high precision data make it the most suitable technique for this
260 study.

261

262 Olivine grains were carefully picked from the groundmass using stainless steel tweezers
263 to avoid any oxygen isotopic contamination. Following the separation, whole-rock chips along
264 with groundmass and olivine-rich fractions of NWA 12320, A 12209 and A-881371 (~2 mg of
265 material per replicate) were loaded into separate wells in a Ni sample holder. Once the fractions
266 were loaded, the holder was placed in the sample chamber and the system was pumped down
267 to a vacuum pressure of $\sim 10^{-7}$ mbar and baked out at around 80 °C overnight to remove any
268 adsorbed moisture from the system.

269

270 Internal obsidian standards were analysed alongside the samples to monitor system
271 performance. Analyses were performed following the standard protocols¹⁵. Briefly, this
272 involved heating the samples with a CO₂ laser (10.6 μm wavelength) in the presence of BrF₅
273 adjusting the beam diameter from 3mm to 1mm in order to achieve a complete reaction.
274 Following the reaction of the sample, the gas is purified over liquid nitrogen temperature traps
275 and KBr at 120°C to remove excess BrF₅ and other reaction products (e.g. SiF₄, F₂, etc) before
276 being expanded into a Thermo Finnigan MAT 253 Dual Inlet Isotope Ratio Mass Spectrometer
277 (IRMS) for isotopic analysis.

278

279 Unlike most other meteorite groups, only one angrite is a recorded fall (Angra Dos
280 Reis)¹. Despite the long terrestrial residence times for angrite meteorites, which range from
281 <0.06 Ma to 0.43 Ma, terrestrial contamination is minor¹. On hand specimen examination,
282 some of the Northwest Africa finds appear to be moderately weathered. This can present a
283 significant problem when attempting to obtain high precision during oxygen isotope analyses.
284 To resolve this issue, leaching of meteoritic finds can remove weathering products, mitigating
285 terrestrial contamination. In this study, we analysed chips of both untreated material and
286 leached material (70 – 170 mg) to determine whether or not the angrites investigated had indeed
287 been affected by terrestrial alteration. This process was conducted using a solution of
288 ethanolamine thioglycollate (EATG), a technique routinely used at the Open University to
289 clean weathered meteorites⁴³. EATG treatment is preferred dilute HCl which can partially
290 remove indigenous glass and feldspathic-rich material. Samples were treated repeatedly until
291 no colour change of the solution was apparent, and then washed with water and then 50/50
292 isopropanol alcohol (IPA). Dried samples are then investigated using the same methodology
293 as the untreated samples.

294

295 For petrographic examination, a small chip of NWA 12320 was embedded within a 1-
296 inch round e-poxy mount and coated using a Safematic CCU-010 Compact Coating Unit (<5
297 μm). The mount was investigated using a Zeiss Crossbeam 550 with an Oxford Instruments
298 Symmetry 2 EBSD detector at The Open University. High-resolution Energy Dispersive X-
299 Ray Spectroscopy (EDS) smart-mapping was collected using an Oxford Instruments Ultim
300 Extreme and an Oxford Instruments Ultim Max detector. The sample was tilted to 70° and an
301 electron beam was used to generate EBSD “maps”, consisting of electron backscatter
302 diffraction patterns (EBSPs) acquired at step sizes ranging from 400 nm. The beam conditions

303 used for both EDS and EBSD analyses comprised an incident beam ranging between 1-2 nA
304 current and a 20 kV accelerating voltage at a working distance of 12 mm.

305

306 **Data availability**

307 All data generated or analysed during this study are either included in the Article or its
308 Supplementary Information.

309

310 **Acknowledgements**

311 Kay Green and Michelle Higgins are thanked for their help in sample preparation. Giulia Degli-
312 Alessandrini is thanked for her assistance with SEM and EBSD analyses. James Malley is
313 thanked for assisting with laser-fluorination work. Graham Ensor is thanked for his help in
314 procuring the NWA angrites. B.G.R-S was supported by a STFC studentship. MA and IAF
315 acknowledge support from STFC grant #ST/T000228/1. Acquisition and analysis of A 12209
316 and A-881371 was supported by JSPS KAKENHI (JP19H01959 to AY, JP19H00726 and
317 JP21K1845 to TM), NIPR (Research Project KP307 to AY), in collaboration with the Belgian
318 Science Policy (Belspo) project BELAM for A 12209. VD, SG and PC thank the FWO-FNRS
319 Excellence of Science (EoS) programme ET-HoME. VD, LP, SG and PC also thank the Belspo
320 project BELAM for past funding. VD thanks FRS-FNRS for support. S.G and P.C
321 acknowledge the support of the VUB Strategic Program.

322

323 **Competing Interests**

324 The authors declare no competing interests

325

326

327 **References**

- 328 1. Keil, K. Angrites, a small but diverse suite of ancient, silica-undersaturated volcanic-
329 plutonic mafic meteorites, and the history of their parent asteroid. *Chem. Erde*. 72.191-
330 218 (2012). <https://doi.org/10.1016/j.chemer.2012.06.002>
- 331 2. Mittlefehldt, D. W., Killgore, M., & Lee, M. T. Petrology and geochemistry of D'Orbigny,
332 geochemistry of Sahara 99555 and the origin of angrites. *Meteorit. Planet Sci.* 37, 345-
333 369 (2002). <https://doi.org/10.1111/j.1945-5100.2002.tb00821.x>
- 334 3. Kruijer, T. S., Kleine, T., & Borg, L. E. The great isotopic dichotomy of the early Solar
335 System. *Nat Astron* (2019). <https://doi.org/10.1038/s41550-019-0959-9>

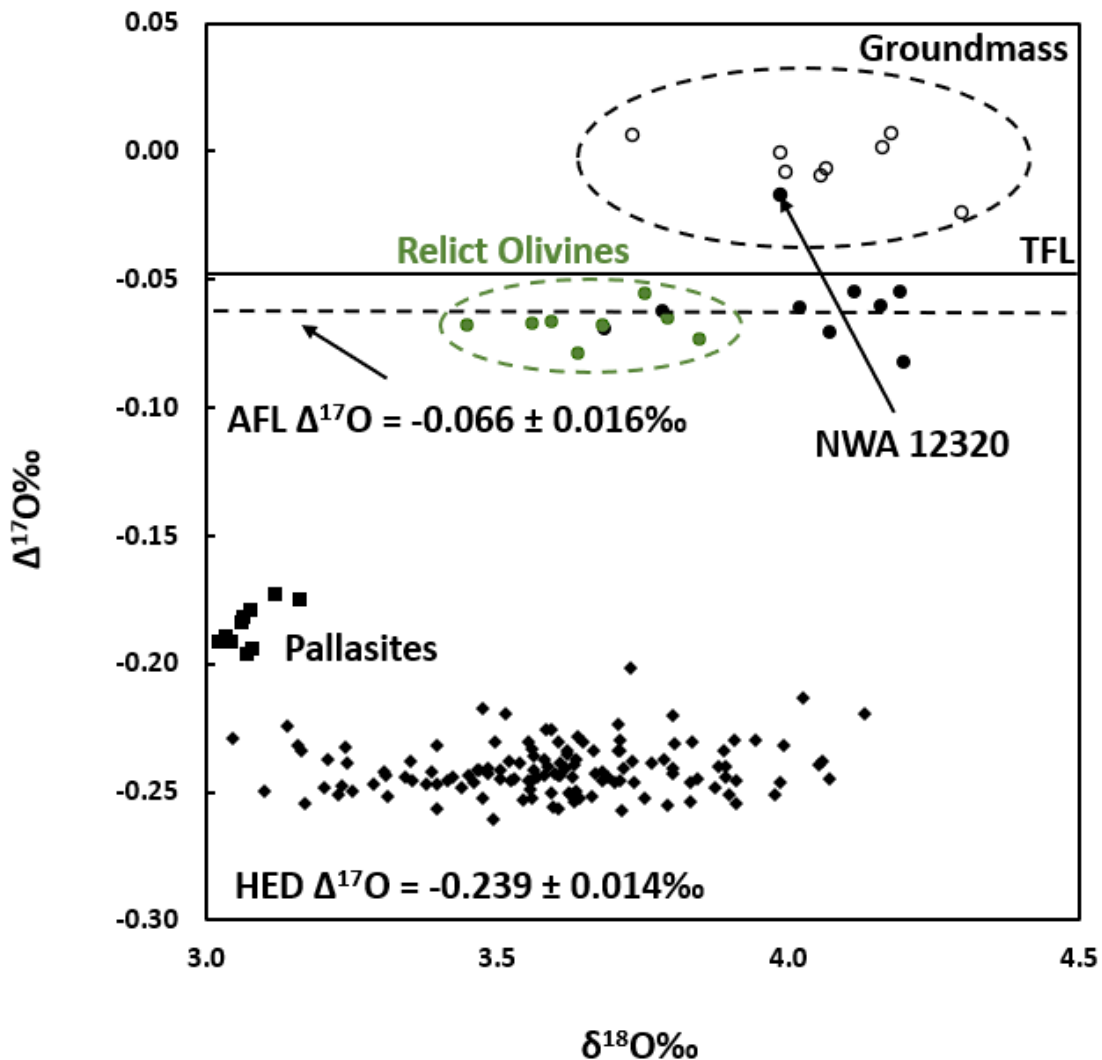
- 336 4. Papike, J. J., Burger, P. V., Bell, A. S., & Shearer, C. K. Mn-Fe systematics in major
337 planetary body reservoirs in the solar system and the positioning of the Angrite Parent
338 Body: A crystal-chemical perspective. *Am. Mineral.* 102, 1759-1762 (2017).
339 <https://doi.org/10.2138/am-2017-6112>
- 340 5. Zhu, K., Moynier, F., Wielandt, D., Larsen, K. K., Barrat, J. A., & Bizzarro, M. Timing and
341 Origin of the Angrite Parent Body Inferred from Cr Isotopes. *Astrophys. J. Lett.* 887:
342 L13 (2019). <https://doi.org/10.3847/2041-8213/ab2044>
- 343 6. Santos, A. R., Agee, C. B., Shearer, C. K., & McCubbin, F. M. Northwest Africa 8535 and
344 Northwest Africa 10463: New insights into the angrite parent body. 47th Lunar and
345 Planetary Science Conference. LPI. Contrib. No. 2590 (2016).
- 346 7. Reger, P. M., Zhang, B., Gannoun, A. M., Regelous, M., Agee, C. B., & Bouvier, A.
347 Chronology of the unique angrite Northwest Africa 10463. 84th Annual Meeting of The
348 Meteoritical Society. LPI. Contrib. No. 2609. (2021).
- 349 8. Greenwood, R. C., Franchi, I. A., Jambon, A., & Buchanan, P. C. Widespread magma oceans
350 on asteroidal bodies in the early Solar System. *Nature.* 435, 916-918 (2005).
351 <https://doi.org/10.1038/nature03612>
- 352 9. Greenwood, R. C., Burbine, T. H., Miller, M. F., & Franchi, I. A. Melting and differentiation
353 of early-formed asteroids: The perspective from high precision oxygen isotope studies.
354 *Chem. Erde.* 77, 1-43 (2017). <https://doi.org/10.1016/j.chemer.2016.09.005>
- 355 10. Scott, E. R. D., & Bottke, W. F. Impact histories of angrites, eucrites and their parent
356 bodies. *Meteorit. Planet. Sci.* 46 (12), 1878-1887 (2011).
357 <http://dx.doi.org/10.1111/j.1945-5100.2011.01301.x>
- 358 11. Jambon, A., Barrat, J. A., Boudouma, O., Fonteilles, M., Badia, D., Göpel, C., & Bohn, M.
359 Mineralogy and petrology of the angrite Northwest Africa 1296. *Meteorit. Planet. Sci.*
360 40, 361-375 (2005). <https://doi.org/10.1111/j.1945-5100.2005.tb00388.x>
- 361 12. Jambon, A., Boudouma, O., Fonteilles, M., Guillou, C. L., Badia, D., & Barrat, J. A.
362 Petrology and mineralogy of the angrite Northwest Africa 1670. *Meteorit. Planet. Sci.*
363 43, 1783-1795 (2008). <https://doi.org/10.1111/j.1945-5100.2008.tb00643.x>
- 364 13. Mikouchi, T., Hasegawa, H., Takenouchi, A., & Kagi, H. Olivine xenocrysts in Asuka-
365 881371 revisited. 46th Lunar and Planetary Science Conference. LPI. Contrib. No. 2065
366 (2015).
- 367 14. Mikouchi, T., Yamaguchi, A., Debaille, V., McKibbin, S., Goderis, S., Pittarello, L., Shirai,
368 N., Hublet, G., Quitté, G., Iizuka, T., Greenwood, R. C., & Claeys, P. Mineralogy of

- 369 olivine xenocrysts in Asuka 12009 angrite. 48th Lunar and Planetary Science
370 Conference. LPI. Contrib. No. 2206 (2017).
- 371 15. Miller, M. F., Franchi, I. A., Sexton, A. S., & Pillinger, C. T. High Precision $\delta^{17}\text{O}$ Isotope
372 Measurements of Oxygen from Silicates and Other Oxides: Method and Applications.
373 RCMS. 13, 1211-1217 (1999). [https://doi.org/10.1002/\(SICI\)1097-
374 0231\(19990715\)13:13%3C1211::AID-RCM576%3E3.0.CO;2-M](https://doi.org/10.1002/(SICI)1097-0231(19990715)13:13%3C1211::AID-RCM576%3E3.0.CO;2-M)
- 375 16. Starkey, N. A., Jackson, C. R. M., Greenwood, R. C., Parman, S., Franchi, I., Jackson, M.,
376 Fritton, J. G., Stuart, F. M., Kurz, M., & Larsen, L. M. Triple oxygen isotopic
377 composition of the high $^3\text{He}/^4\text{He}$ mantle. *Geochim Cosmochim. Acta.* 176, 227-238
378 (2016). <https://doi.org/10.1016/j.gca.2015.12.027>
- 379 17. Trepmann, C. A., Renner, J., & Druiventak, A. Experimental deformation and
380 recrystallization of olivine – processes and timescales of damage healing during
381 postseismic relaxation at mantle depths. *Solid Earth Discuss.* 5, 463-524 (2013).
382 <https://doi.org/10.5194/se-4-423-2013>
- 383 18. Janots, E., Gnos, E., Hofmann, B. A., Greenwood, R. C., Franchi, I. A., Bermingham, K.,
384 & Netwing, V. Jiddat al Harris 556: A howardite impact melt breccia with an H
385 chondrite component. *Meteorit. Planet Sci.* 47, 1558-1574 (2012).
386 <https://doi.org/10.1111/j.1945-5100.2012.01419.x>
- 387 19. Janots, E., Gnos, E., Hofmann, B. A., Greenwood, R. C., Franchi, I. A., & Bischoff, A.
388 Jiddat al Harris 422: A ureilite with an extremely high degree of shock melting.
389 *Meteorit. Planet Sci.* 46, 134-148 (2011). [https://doi.org/10.1111/j.1945-
390 5100.2010.01161.x](https://doi.org/10.1111/j.1945-5100.2010.01161.x)
- 391 20. Nazarov, M. A., Brandstätter, F., & Kurat, G. Angrite-like clasts from the Erevan
392 howardite. LPI. Contrib. No. 1033 (1995).
- 393 21. Cohen, B. A., Goodrich, C. A., & Keil, K. Feldspathic clast populations in polymict
394 ureilites: Stalking the missing basalts from the ureilite parent body. *Geochim
395 Cosmochim. Acta.* 64 (20), 4249-4266 (2004).
396 <https://doi.org/10.1016/j.gca.2004.01.027>
- 397 22. Kita, N. T., Ikeda, Y., Togashi, S., Liu, Y., Morishita, Y., & Weisberg, M. K. Origin of
398 ureilites, inferred from a SIMS oxygen isotopic and trace element study of clasts in the
399 Dar al Gani polymict ureilites. *Geochim Cosmochim. Acta.* 68 (20), 4213-4235 (2004).
400 <https://doi.org/10.1016/j.gca.2004.03.020>
- 401 23. Zhang, A. C., Kawasaki, N., Kuroda, M., Li, Y., Wang, H. P., Bai, X. N., Sakamoto, N.,
402 Yin, Q. Z., Yurimoto, H. Unique angrite-like fragments in a CH3 chondrite reveal a

- 403 new basaltic planetesimal. *Geochim Cosmochim. Acta.* 275, 48-63 (2020).
404 <https://doi.org/10.1016/j.gca.2020.02.014>
- 405 24. Jambon, A., Baghdadi, B., & Barrat, J. A. Peridotitic angrites are chimerolites. 43rd Lunar
406 and Planetary Science Conference. LPI. Contrib. No. 1758 (2012).
- 407 25. Sarafian, A. R., Hauri, E. H., McCubbin, M., Lapen, T. J., Berger, E. L., Nielson, S. G.,
408 Marschall, H. R., Gaetani, G. A., Righter, K., & Sarafian E. Early accretion of water
409 and volatile elements to the inner Solar System: evidence from angrites. *Philos. Trans.*
410 *R. Soc.* 375. <https://doi.org/10.1098/rsta.2016.0209>
- 411 26. Deligny, C., Füre, E., & Deloule E. Origin and timing of volatile delivery (N, H) to the
412 angrite parent body: Constraints from in situ analyses of melt inclusions. *Geochim*
413 *Cosmochim. Acta.* 313, 243-256 (2021). <https://doi.org/10.1016/j.gca.2021.07.038>
- 414 27. Greenwood, R. C., Burbine, T. H., & Franchi, I. A. Linking asteroids and meteorites to the
415 primordial planetesimal population. *Geochim Cosmochim. Acta.* 277, 377-406 (2020).
416 <https://doi.org/10.1016/j.gca.2020.02.004>
- 417 28. Clayton, R. N., Mayeda, T. K., Goswami, J. N., & Olsen, E. J. Oxygen isotope studies of
418 ordinary chondrites. *Geochim Cosmochim. Acta.* 55, 2317-2337 (1991).
419 [https://doi.org/10.1016/0016-7037\(91\)90107-G](https://doi.org/10.1016/0016-7037(91)90107-G)
- 420 29. Riches, A. J. V., Day, J. M. D. Walker, R. J., Simonetti, A., Liu, Y., Neal, C. R., & Taylor,
421 L. A. Rhenium-osmium isotope and highly-siderophile-element abundance systematics
422 of angrite meteorites. *Earth Planet Sci. Lett.* 353-354, 208-218 (2012).
423 <https://doi.org/10.1016/j.epsl.2012.08.006>
- 424 30. Steenstra, E. S., Sitabi, A. B., Lin, T. H., Rai, N., Knibbe, J. S., Berndt, J., Matveev, S., &
425 Westrenen, W. V. The effect of melt composition on metal-silicate partitioning of
426 siderophile elements and constrains on core formation in the angrite parent body.
427 *Geochim Cosmochim. Acta.* 212, 62-83 (2017).
428 <https://doi.org/10.1016/j.gca.2017.05.034>
- 429 31. Isa, J., Rubin, A. E., Wasson, J. T. R-chondrite bulk-chemical compositions and diverse
430 oxides: Implications for parent-body processes. *Geochim Cosmochim. Acta.* 124, 131-
431 151 (2014). <https://doi.org/10.1016/j.gca.2013.09.018>
- 432 32. Morbidelli, A., Walsh, K. J., O'Brien, D. P., Minton, D. A., & Bottke, W. F. The dynamical
433 evolution of the asteroid belt. In *Asteroids IV*. 493-507, (2015).
434 <https://doi.org/10.48550/arXiv.1501.06204>
- 435 33. Greenwood, R. C., Barrat J-A., Miller M. F., Anand A., Dauphas N., Franchi I. A., Sillard
436 P. and Starkey N. A. Oxygen isotopic evidence for accretion of Earth's water before a

- 437 high-energy Moon-forming giant impact. *Sci Adv.* 4, 3 (2018).
438 <https://doi.org/10.1126/sciadv.aao5928>
- 439 34. Qin, L. & Carlson, R. W. Nucleosynthetic isotope anomalies and their cosmochemical
440 significance. *Geochemical J.* 50, 43-65 (2016).
441 <https://doi.org/10.2343/geochemj.2.0401>
- 442 35. Johnson, B. C., Walsh, K. J., Minton, D. A., Krot, A. N., & Levison, H. F. Timing of the
443 formation and migration of giant planets as constrained by CB chondrites. *Sci Adv*, 2,
444 12 (2016). <https://doi.org/10.1126/sciadv.1601658>
- 445 36. Raymond, S. N., Izidoro, A., & Morbidelli, A. Solar System formation in the context of
446 extra-solar planets. *Planetary Astrobiology.* 287-234 (2020).
447 <https://doi.org/10.48550/arXiv.1812.01033>
- 448 37. Walsh, K., Morbidelli, A., Raymond, S., O'Brien, D. P., & Mandell, A. M. A low mass for
449 Mars from Jupiter's early gas-driven migration. *Nature.* 475, 206–209 (2011).
450 <https://doi.org/10.1038/nature10201>
- 451 38. Connelly, J. N., Bizzaro, M., Krot, Nordlund, A., Wielandt, D., & Ivanova, M. A. The
452 absolute chronology and thermal processing of solids in the solar protoplanetary disk.
453 *Science.* 338, 651-655 (2012). <https://doi.org/10.1126/science.1226919>
- 454 39. Wang, H., Weiss, B. P., Bai, X. N., Downey, B. G., Wang, J., Wang, J., Suavet, C., Fu, R.
455 R., & Zucolotto, M. E. Lifetime of the solar nebula constrained by meteorite
456 paleomagnetism. *Science* 355, 623-627 (2017).
457 <https://doi.org/10.1126/science.aaf5043>
- 458 40. Brennecka, G. A., & Wadhwa, M. Uranium isotope compositions of the basaltic angrite
459 meteorites and the chronological implications for the early Solar System. *Proc. Natl.*
460 *Acad. Sci.* 109, 9299-9303 (2012). <https://doi.org/10.1073/pnas.1114043109>
- 461 41. Clayton, R. N., & Mayeda, T. K. Oxygen isotope studies of Achondrites. *Geochim*
462 *Cosmochim. Acta.* 60, 1999-2017 (1996). [https://doi.org/10.1016/0016-](https://doi.org/10.1016/0016-7037(96)00074-9)
463 [7037\(96\)00074-9](https://doi.org/10.1016/0016-7037(96)00074-9)
- 464 42. Miller, M. F. Isotopic fractionation and the quantification of ^{17}O anomalies in the oxygen
465 three-isotope system: an appraisal and geochemical significance. *Geochim*
466 *Cosmochim. Acta.* 66, 1881–1889 (2002). [https://doi.org/10.1016/S0016-](https://doi.org/10.1016/S0016-7037(02)00832-3)
467 [7037\(02\)00832-3](https://doi.org/10.1016/S0016-7037(02)00832-3)
- 468 43. Martins, Z., Hofmann, B. A., Gnos, E., Greenwood, R. C., Verchovsky, A., Franchi, I., Jull,
469 A. J. T., Botta, O., Glavin, D. P., Dworkin, J. P., Ehrenfreund, P. Amino acid
470 composition, petrology, geochemistry, ^{14}C terrestrial age and oxygen isotopes of the

471 Shisr 033 CR chondrite. *Meteorit. Planet. Sci.* 42 (9), 1581-1595 (2010).
 472 <https://doi.org/10.1111/j.1945-5100.2007.tb00592.x>

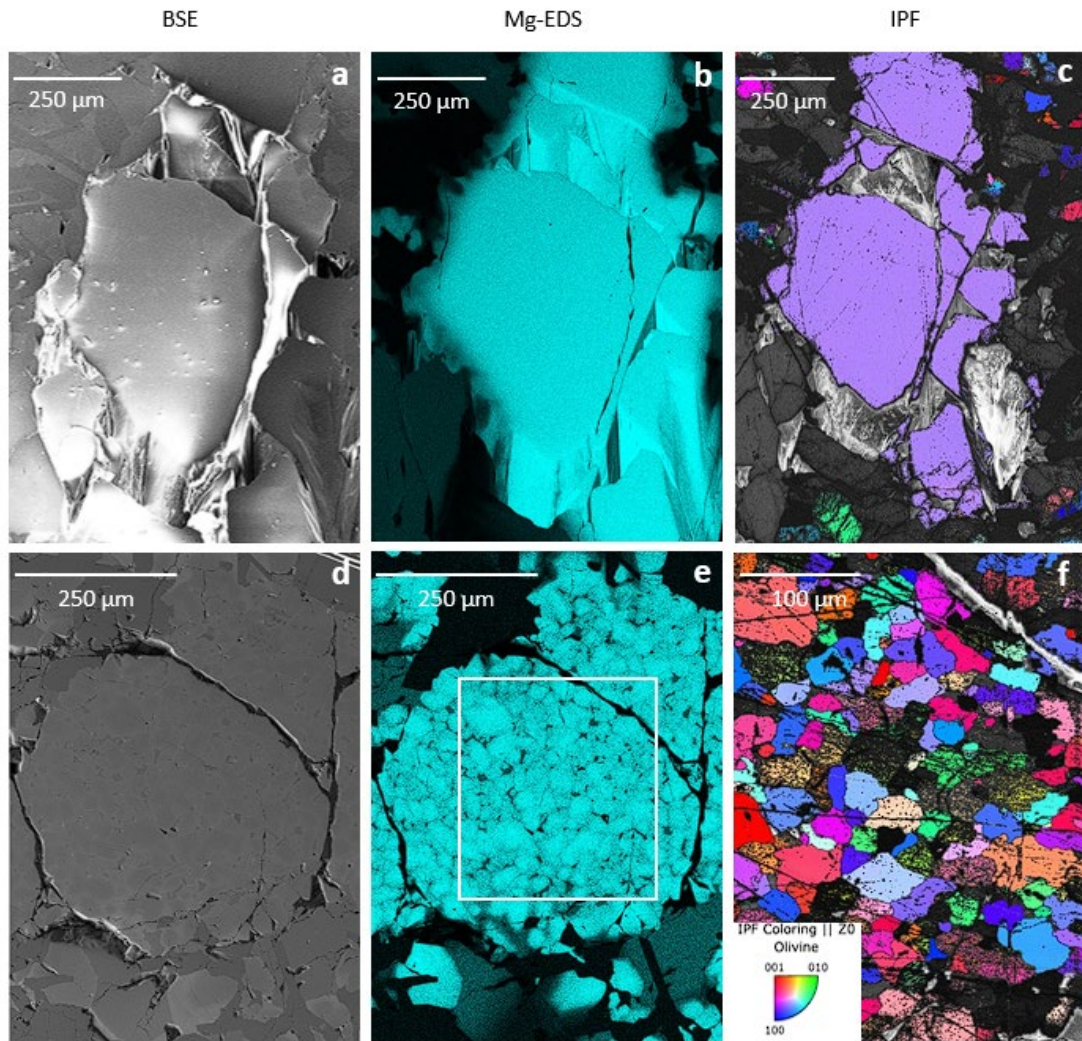


473
 474 *Figure 1: Triple oxygen isotope systematics for angrites, pallasites and HEDs. In this*
 475 *diagram, we show our angrite data in relation to a TFL line (-0.048 ± 0.020) that has been*
 476 *calibrated using a suite of 195 terrestrial samples run under identical conditions to the angrites*
 477 *in this study and calculated using the same slope factor (0.5247) (see text for further details).*
 478 *Relict olivines (green closed circles) from A 12209, A-881371 and NWA 12320 display similar*
 479 *values to bulk angrites (black closed circles) and fall within the newly-defined AFL ($\Delta^{17}\text{O} -$*
 480 *0.066 ± 0.016 ‰), while groundmass fractions (open black circles) yield more positive $\Delta^{17}\text{O}$*
 481 *values. This discrepancy in at least three angritic meteorites, suggests contributions from*
 482 *unique parent bodies for both the olivine and groundmass fractions, requiring early mixing of*

483 *planetary reservoirs on the angrite parent body. The angrite meteorites are well resolved from*
 484 *both pallasite meteorites (black triangles) and howardite-eucrite-diogenite (HED) meteorites*
 485 *(black squares)⁸. Cross represents 2SD uncertainty⁴².*

486

487



488

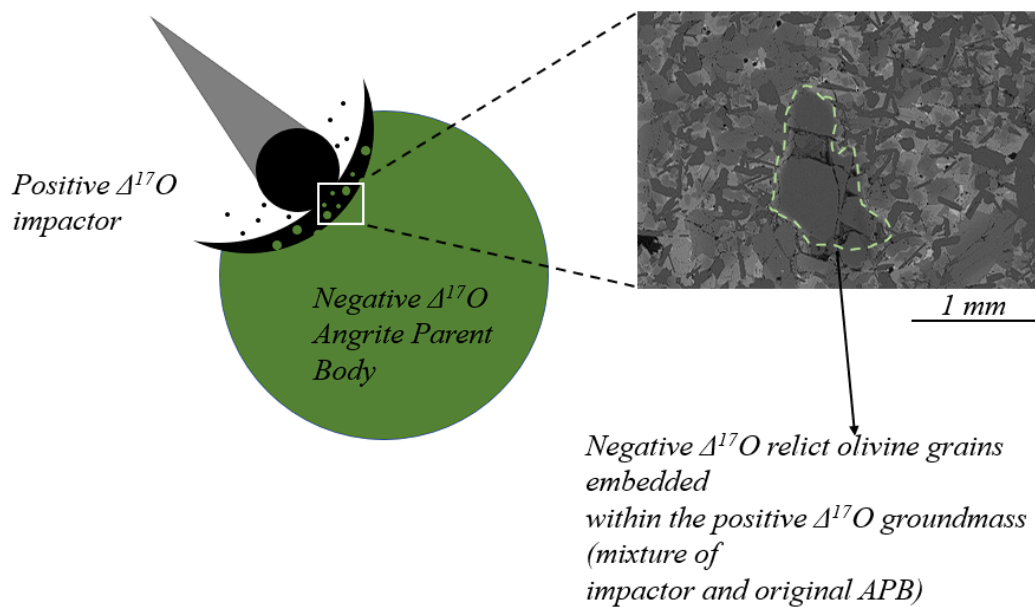
489

490 **Figure 2: Chemical and structural characterisation of relict olivine grains in NWA 12320.**
 491 *Two populations of olivine are observed within the sample as shown by backscatter electron*
 492 *(BSE) imaging (a & d). Both of which are chemically heterogenous, as evidenced by*
 493 *magnesium energy dispersive (Mg-EDS) imaging (b & e). Inverse pole figure (IPF) images*
 494 *demonstrate the difference between non-recrystallised relict grains (c), displaying a single*
 495 *orientation (purple), versus the recrystallized relict grains (f), displaying multiple crystallites*
 496 *with differing orientations (multi-colour grains). Given the low state of deformation within*

497 *both the undeformed olivine grains, as well as the majority of angrite meteorites, olivine*
498 *recrystallization for a subset of grains must have occurred prior to crystallization of the bulk*
499 *sample, suggesting that the olivine are relict material that survived impact melting.*

500

501



502

503

504 *Figure 3 – A schematic depicting a possible scenario which causes the oxygen isotopic*
505 *disequilibrium in the quenched angrite meteorites. An impactor with a positive oxygen*
506 *isotopic composition, collides with the angrite parent body (APB). Mixing of the two separate*
507 *bodies occurs and relict olivine grains of the APB are affected by high temperature events.*
508 *Plutonic and dunitic angrites escape shock deformation and isotopic mixing due to their depth/*
509 *distance from the impact site on the APB or due to being molten during the time of impact*
510 *mixing. Backscatter electron (BSE) image of the relict olivine grain is the grain depicted in*
511 *Figure 2a-c.*

512

513

514

515

516